Published in final edited form as:
J Comp Neurol. 2011 January 1; 519(1): 6–20. doi:10.1002/cne.22503.

Neurogenic Hippocampal Targets of Deep Brain Stimulation

Juan M. Encinas[1,#], **Clement Hamani**[2,#], **Andres M. Lozano**[2], and **Grigori Enikolopov**[1]
[1]Cold Spring Harbor Laboratory, Cold Spring Harbor, NY 11724

[2]Division of Neurosurgery, Toronto Western Hospital, Toronto, Ontario, M5T 2S8, Canada

Abstract

Deep brain stimulation (DBS) is being used to treat movement, neurological, and psychiatric disorders; it has been recently successfully applied to patients with treatment-resistant depression or in minimally conscious state. In addition to its clinical importance, DBS presents a powerful approach to target specific neural circuits and determine the functional relationship between the components of these circuits. We examined the effect of high frequency stimulation of a crucial component of the limbic circuitry, the anterior thalamic nuclei (ATN), on the generation of new neurons in the dentate gyrus (DG) of the hippocampus, another component of the same circuitry. Adult hippocampal neurogenesis emerges as a strong correlate of antidepressant treatments; however, in most cases the progenitor cell population targeted by a specific treatment is not known. Using reporter mouse lines designed to quantify changes in selected classes of neural progenitors, we found that high frequency stimulation of the ATN increases symmetric divisions of a defined class of neural progenitors in the DG; this effect is later manifested as an increased number of new neurons. The affected class of neural progenitors is also affected by the antidepressant fluoxetine (Prozac) and physical exercise (running). This indicates that neurogenic stimuli of different nature can converge on the same neurogenic target in the DG. Our results also suggest that hippocampal neurogenesis may be used as a sensitive indicator of the limbic circuitry activation induced by DBS.

Keywords

Deep brain stimulation; anterior thalamus; adult neurogenesis; transgenic mice; stem cells

Introduction

Deep brain stimulation (DBS) has proven to be effective in treating a range of neurological disorders including Parkinson's disease, essential tremor, and dystonia and pain (Lozano and Hamani, 2004; Wichmann and Delong, 2006). Recently, beneficial effects of DBS have been reported for Tourette's syndrome and intractable epilepsy (Andrade et al., 2006; Houeto et al., 2005; Kerrigan et al., 2004; Vandewalle et al., 1999). Furthermore, DBS is being examined in regards to psychiatric disorders, such as obsessive-compulsive disorder (Gabriels et al., 2003; Greenberg et al., 2010; Kopell et al., 2004) and treatment-resistant depression (Bewernick et al.,; Jimenez et al., 2007; Lozano et al., 2008; Malone et al., 2009; Mayberg et al., 2005; Schlaepfer et al., 2008). Moreover, DBS may also prove useful in recovery from minimally conscious state (Schiff et al., 2007; Yamamoto et al., 2002) and for

Corresponding author: Grigori Enikolopov, Cold Spring Harbor Laboratory, 1 Bungtown Road, Cold Spring Harbor, NY 11724, enikolop@cshl.edu.
[#]equal contribution

memory enhancement (Hamani et al., 2008). The efficacy of the DBS critically depends on targeting the brain regions and functional circuits involved in a specific disorder.

Here, we have focused on the limbic system circuitry which is involved in complex behavioral reactions and which includes several brain regions that have been successfully exploited by DBS for therapeutic benefits. Hippocampus is a critical component of the limbic circuitry and is distinguished among other regions of the brain by persistent production of new neurons. Hippocampal neurogenesis emerges as a strong correlate of cognitive and emotional processes and its levels change in response to a wide array of stimuli, including enriched environment, learning, stress, seizures, and antidepressants; moreover, it may be necessary for the action of antidepressants, hippocampal synaptic plasticity, and complex behaviors (Drew and Hen, 2007; Santarelli et al., 2003; Warner-Schmidt and Duman, 2006; Zhao et al., 2008). A major unresolved issue in hippocampal neurogenesis is the identification of cells that are targeted by neurogenic stimuli. Particular targets (e.g., neural stem or early progenitor cells undergoing symmetric or asymmetric divisions) would imply specific mechanisms and implicate specific neuronal circuits mediating the action of the stimulus; moreover, convergence of dissimilar stimuli on the same targets may point to commonalities in the circuits activated by such stimuli. We used a reporter transgenic mouse line (Nestin-CFPnuc; (Encinas et al., 2006; Enikolopov and Overstreet-Wadiche, 2007) to determine the neurogenic target of DBS of the anterior thalamic nuclei (ATN) and show that this treatment affects the same class of hippocampal neural progenitors as fluoxetine and physical exercise.

Materials and Methods

Animals

Mice were housed in a standard light- and temperature-controlled environment (12 hr light/dark cycle; light on at 7:00 a.m.; t=21±2°) and access to food and water ad libitum. All procedures were approved by Animal Care and Use Committees of Cold Spring Harbor Laboratory, and the protocols are in accordance with Guidelines for the Use and Treatment of Animals by National Institutes of Health. Age-matched 13-week old C57BL/6 mice were used for the initial series of experiments to determine the specificity of the ATN electrical stimulation on cell proliferation in the dentate gyrus (DG). In the main series of experiments, aged-matched 2-month old Nestin-CFPnuc transgenic animals were used. In these animals, the transgene contained cDNA of the enhanced version of CFP fused to a nuclear localization signal for simian virus 40 (SV40), controlled by the 5.8-kb fragment of the promoter region of the Nestin gene, 1.8-kb fragment containing the second intron of the Nestin gene, and polyadenylation sequences from SV40 and cloned into the pBSM13^{+} vector. CFPnuc cDNA was placed between the Nestin promoter and intron sequences, matching their arrangement in the Nestin gene. The transgene and the animals are described in (Mignone et al., 2004) and (Encinas et al., 2006). The pattern of the fluorescent reporter expression in Nestin-CFPnuc mice is the same as in Nestin-GFP mice (Encinas et al., 2006); in turn, the pattern of transgene expression in Nestin-GFP mice closely corresponds to the pattern of expression of endogenous Nestin (Mignone et al., 2004).

Surgery

Animals were anesthetized with a solution of ketamine/xylazine (100/10 mg/kg) injected intraperitoneally and had their heads fixed in a stereotactic instrument (Model 900, David Kopf Instruments, Tujunga, CA). For electrical stimulation, we used polymide insulated stainless steel electrodes with diameter of 125 μm and an exposed tip of 0.5 mm. The electrodes were bilaterally implanted into the anterior thalamic nuclear complex at the following stereotactic coordinates relative to the bregma: anteroposterior -0.8 mm, medial-

lateral ± 0.7 mm, dorsoventral 3.5 mm (Franklin and Paxinos, 1997). As a control for target specificity, a group of animals was implanted with electrodes in the frontal associative area of the cortex (FrA; anteroposterior -2.9 mm, medial-lateral ± 0.7 mm, dorsoventral 1.8 mm (Franklin and Paxinos, 1997). This region was selected as the hippocampus is not one of its major projections and it is far enough from the ATN so that an effect due to current spread would be unlikely.

In all experiments, thalamic electrodes were used as cathodes and a needle inserted in the neck muscle was used as the anode. This monopolar configuration was chosen as it is the most common stimulation setting used in clinical practice. Once the electrodes were in place, stimulation was conducted for 1 hr with a Medtronic 3628 screener (Medtronic Inc., Minneapolis, MN) at the following parameters: 2.5 V, 90 μseconds of pulse width, and frequency of either 10Hz (low frequency stimulation; LF group) or 130Hz (high frequency stimulation; HF group). These frequencies were selected based on our control experiments and previous studies (Toda et al., 2008), which suggested that stimulation above 50Hz induces neurogenesis. Sham-treated control animals were anesthetized and had electrodes implanted into the ATN but did not receive stimulation (non stimulated; NF group). After the procedures, the electrodes were removed, the surgical planes were closed and the animals were allowed to recover.

In the series of experiments with C57BL/6 mice, 4 animals received ATN LF, 5 received FrA LF, 4 received ATN HF, and 3 received FrA HF. For the series with Nestin-CFPnuc mice, 10 animals received ATN LF, 10 received ATN HF, and 9 animals were not stimulated (NF). All mice were injected 3 times with 5-bromo-2′-deoxyuridine (BrdU) 72 hr after the surgery (150mg/kg each injection, in 3 hr intervals) and sacrificed 24 hr or 30 days after the first BrdU injection (Fig 1A). The intervals were suggested by previous experiments which showed a lag between the stimulation and the increase in neurogenesis (Toda et al., 2008). The brain slices were analyzed for BrdU staining using a standard DAB immunostaining protocol (see below) and lightly counterstained with Toluidine Blue (Sigma). For all animals the correct positioning of the electrode was verified *post mortem* by tracking the path of the electrode in the brain slices (Figs. 1B, C and 2A, B). Analysis of the data was limited to the animals for which the correct placement and targeted brain regions were confirmed. With the selected settings, it is likely that all subnuclei of the anterior thalamic complex (anteromedial, anteroventral, and anterodorsal) and adjacent structures were being influenced by stimulation; note that this is also the case in humans, as the regions influenced by anterior thalamic stimulation are still unclear.

Antibody characterization

Primary antibodies used in this study are listed in Table 1. Information on the antibodies is derived from the manufacturers' description and our own data.

According to the manufacturer, the antibody to BrdU (AbD Serotec; Realeigh, NC) recognizes BrdU incorporated into single stranded DNA or attached to a protein carrier as well as free BrdU. The pattern of staining is restricted to the cell nucleus and is not present when BrdU has not been administered to the cells or animals analyzed.

The antibody to glial fibrillary acidic protein (GFAP; Sigma-Aldrich; St. Louis, MO) recognizes GFAP in the cytoplasm of astrocytes, radial glia, Bergmann glia, gliomas and other glial cell derived tumors and does not stain non-glial cells. According to the manufacturer, it recognizes a single band of 46kD corresponding to the molecular weight of GFAP in immunoblots of whole cell extract of rat brain.

The antibody to green fluorescent protein (GFP, Aves Laboratories; Tigard, OR) recognizes GFP in tissue from GFP-expressing transgenic mice. The signal is present in the same cells where expression of GFP or CFPnuc is detected (driven by regulatory elements of Nestin gene in our case), but not in others. Furthermore, the signal is not detected in non-transgenic mice. In immunoblots of transgenic mice tissues, the antibody recognizes a single band of 27kD, corresponding to the molecular weight of GFP.

The antibody to NeuN (Chemicon-Millipore; Billerica, MA) recognizes the DNA-binding neuron-specific protein NeuN, which is present in most neuronal cell types of vertebrate CNS and PNS. NeuN staining is restricted to neuronal nuclei and perikarya. Some neuronal types, such as INL retinal cells, Cajal-Retzius cells, Purkinje cells, inferior olivary and dentate nucleus neurons and sympathetic ganglion cells fail to be recognized by the antibody. According to the manufacturer, it recognizes 2-3 bands in the 46-48 kD range and a weaker one at ~66 kD on immunoblots. It does not stain non-neuronal cell types.

The antibody to anti-polysialic neural cell adhesion molecule (PSA-NCAM) (Chemicon-Millipore) reacts with polysialic acid (PSA), an alpha 2-8 linked neuraminic acid polymer. In vertebrates, PSA is linked to neural cell adhesion molecule (NCAM, CD56), in bacteria it is associated with the capsula of meningococcus strain group B. In the rodent tissues it stains the membrane of young neurons or neuroblasts. It does not stain non-neuronal cell types. According to the manufacturer, the antibody recognizes a single band of ~200kD in immunoblots of developing rodent brains.

The following secondary antibodies were used: biotin-conjugated donkey anti-rat (Vector Laboratories, Burlingame, CA) at 1:200; AlexaFluor 488 goat anti-chicken (Molecular Probes, Willow Creek Road, Eugene, OR) at 1:500; AlexaFluor 594 goat anti-mouse (Molecular Probes) at 1:500; AlexaFluor 568 goat anti-rat (Molecular Probes) at 1:500; Cy5 goat anti-chicken (Jackson Immunoresearch, West Grove, PA) at 1:500; and Texas Red donkey anti-chicken (Jackson Immunoresearch) at 1:500.

Immunohistochemistry

Mice were fixed by transcardial perfusion with 30 ml of 4% (w/v) paraformaldehyde in phosphate-buffered saline (PBS), pH 7.4. The brains were removed, cut longitudinally into two hemispheres and postfixed, with the same fixative, for 3 hrs at room temperature, then transferred to PBS and kept at 4°C. Serial 50-μm thick sagittal sections were cut using Vibratome 1500 (Vibratome, St. Louis, MO). Immunostaining was carried out following a standard procedure: The sections were incubated with blocking and permeabilization solution (PBS containing 0.2 % Triton-100X and 3% bovine serum albumin) for 1hr at room temperature, and then incubated overnight with the primary antibodies (diluted in the same solution) at 4°C. For staining with chromogen 3,3′-diaminobenzidine (DAB), after thorough washing with PBS the sections were incubated with biotinylated secondary antibodies in PBS for 1 hr at room temperature. After washing, the sections were incubated with peroxidase-linked ABC (Vector Labs). The peroxidase activity was demonstrated using the Fast 3,3′-diaminobenzidine tetrahydrochloride with metal enhancer tablet set (Sigma-Aldrich, St Louis, MO). For immunofluorescence, after thorough washing with PBS the sections were incubated with fluorochrome-conjugated secondary antibodies in PBS for 1 hr at room temperature. After washing with PBS, the sections were mounted on gelatin coated slides with DakoCytomation Fluorescent Mounting Medium (DakoCytomation, Carpinteria, CA). Those sections destined to the analysis of BrdU incorporation were treated, before the immunostaining procedure, with 2M HCl for 30 min at 55°C, rinsed with PBS, treated with 1mM sodium tetraborate for 10 min at room temperature, and then rinsed with PBS. The CFPnuc signal from the transgenic mice was detected with an antibody against GFP for

enhancement and better visualization. Primary and secondary antibodies are described above.

Image capture

All fluorescence immunostaining images were collected employing a laser scanning microscope LSM 510 (Carl Zeiss, Thornwood, NY) and the corresponding manufacturer's software. All images shown correspond to 15 μm z-stacks, except the main picture of the orthogonal projections of Fig. 6, which correspond to 1.5 μm focal planes. DAB-immunostained images from Fig. 1 were captured with a bright field microscope (Carl Zeiss). All images were imported into Adobe Photoshop 7.0 (Adobe Systems Incorporated, San Jose, CA) in *tiff* format. Red fluorescence signal was replaced by magenta; brightness, contrast, and background were adjusted using the “brightness and contrast” controls from the “image/adjustment” set of options.

Quantification

Quantitative analysis of cell populations was performed by means of design-based (assumption free, unbiased) stereology (Encinas and Enikolopov, 2008; Peterson, 1999). Slices were collected using systematic-random sampling. One brain hemisphere was randomly selected per animal. The hemisphere was sliced sagittally in a lateral-to-medial direction, from the beginning of the lateral ventricle to the middle line, thus including the entire DG. The 50 μm slices were collected in 6 parallel sets, each set consisting of 12 slices, each slice 300 μm apart from the next. For cell quantification in the DG, all cells of each type described in the Results were counted in every slice, using the 63× objective. Adjacent z-stacks of the entire thickness of the section were collected by means of confocal microscopy, with the exception of the results in Fig. 1 which correspond to DAB-staining (see the “Image capture” section). Then, all of the cells in the section were counted, excluding those in the uppermost focal plane, and assigned to their corresponding category ($BrdU^+$; QNP; ANP; $BrdU^+$QNP; $BrdU^+$ANP; PSA-$NCAM^+$; $BrdU^+NeuN^+$, etc). The number of cells (for each category) from all the slices from one set was added up together and multiplied by 6 (the number of sets of slices per animal), the value representing the total number of cells per hemisphere; these numbers are given in the Results section. In the proliferation study, one set of slices was used to determine the numbers of BrdU+ cells (these sections were also stained for CFP for accurate anatomical resolution and measurement of the volume of the SVZ); another set was used to determine the total number of Nestin-CFPnuc+ (QNPs and ANPs together), using GFAP staining to distinguish between the two cell types; another set of slices was used for BrdU+QNPs and BrdU+ANPs staining using triple labeling for BrdU, CFP, GFAP; yet another set was used for PSA-NCAM immunostaining.

To evaluate the accuracy of cell counts, we determined the size of stem and progenitor cells' nuclei, which are clearly defined by the CFP expression. The values are 7.425 ± 1.000 μm for the NF group, 7. 050 ± 0.902 μm for the LF group, and 7.325 ± 0.990 μm for the HF group, with the thickness of sections being 50 μm for all specimens. Thus, our “real” to observed counts ratio (Abercrombie correction factor) (Guillery, 2002) are 0.87 for the NF, 0.88 for the LF, and 0.87 for the HF groups. These values indicate a high level of accuracy of our calculations and further indicate that different types of treatments did not affect the size of the counted objects (the nuclei). The volume of the reference structure, comprised of the granule cells layer (GCL) and the subgranular cell zone (SGZ) was calculated using the Cavalieri-point method, using a set of slices immunostained for NeuN and CFP. In the cell differentiation study, one set of slices was stained for BrdU and NeuN to quantify the $BrdU^+$ and $NeuN^+BrdU^+$ cells (each $BrdU^+$ cell was analyzed through orthogonal projections to test for co-localization with NeuN), and another set was analyzed for CFP and GFAP

labeling to quantify QNPs and ANPs. These cell types were counted as described above for the DG. A separate set of slices was immunostained for NeuN and CFP to measure the volume of the GCL, including the SGZ. No differences were found in the volume of the GCL+SGZ in any group.

Statistical analysis

Statistical analysis was performed employing Stastistica (StatSoft, Tulsa, Oklahoma) software. The data from the wild type animals (LF and HF groups) were analyzed by the Student's test. All data sets from the transgenic Nestin-CFPnuc mice (NF, LF, and HF groups) were tested for normal distribution and for homogeneity of the variances (using Levene's test) prior to analysis with a one-way two-tailed ANOVA. When significant differences were found ($p \leq 0.05$), post-hoc analysis with the Tukey-HSD test (high significance difference) followed, to find out where the differences were and what was its associated p value. These p values are the ones offered throughout the results section. Graphs were plotted using Sigmaplot 8.0 (SPSS Inc., Chicago, IL), the vertical bars show the mean with the standard error of the mean (s.e.m), and the black dots show the individual data for each animal.

Results

High frequency stimulation of the ATN increases cell proliferation in the adult mouse hippocampus

We first examined whether stimulation of the ATN can increase cell proliferation in the neurogenic zones of the adult mouse brain. Such effect has been recently demonstrated in rats (Toda et al., 2008) and we followed a similar experimental paradigm to determine the effect of stimulation on cell proliferation, as measured by BrdU incorporation, in the subgranular zone of the DG (SGZ) and the subventricular zone (SVZ), two major zones of adult neurogenesis. We compared the groups of animals subjected to surgery and bilateral electrode insertion in the ATN after subjecting them to low frequency (10Hz, LF group) and high frequency (130Hz, HF group) electric stimulation (note that in these experiments all subnuclei of the anterior thalamic complex are likely to be stimulated); an additional group of animals received stimulation of the frontal associative area of the cortex (FrA). There was a significant increase (41%) in the number of BrdU-labeled cells in the DG of the ATN HF group compared to the ATN LF group and no difference between the ATN LF and the FrA groups (Fig. 1D-I). Furthermore, there was no difference in cell division in the SVZ of either group. These experiments demonstrate the ability of high frequency stimulation, directed at a component of the limbic circuit, to increase hippocampal neurogenesis.

High frequency stimulation of the ATN increases the number of amplifying neural progenitors in the DG

The observations of increased cell proliferation after high frequency stimulation do not reveal the identity of the dividing cells: the changes may reflect increased symmetric or asymmetric division of stem cells, early progenitors, changes in advanced progenitors (neuroblasts), immature neurons, or some combination thereof. We addressed this issue by applying an approach that we developed for quantitative evaluation of changes in various compartments of the neuronal differentiation cascade (Encinas and Enikolopov, 2008; Enikolopov and Overstreet-Wadiche, 2007). This approach makes use of a reporter transgenic mouse line in which nuclei of stem and early progenitor cells are labeled by cyan fluorescent protein which is fused to a nuclear localization signal (CFPnuc) and expressed under the control of the Nestin gene regulatory elements (Nestin-CFPnuc mice). Nuclear localization of the fluorescent signal reduces the complexity of the distribution pattern of neurogenic cells allowing enumeration of changes in selected groups of neuronal precursors

with great accuracy and precision. We have used this approach to determine the essential steps in the neurogenesis cascade in the DG and identify the cell populations in the DG targeted by the selective serotonin reuptake inhibitor (SSRI) fluoxetine (Prozac) (Encinas et al., 2006), physical activity (Hodge et al., 2008), ablation of dopaminergic neurons (Park and Enikolopov, 2010), and brain trauma (Gao et al., 2009).

We first compared the animals that received low frequency (LF group), high frequency (HF group), or no stimulation (NF group) of the ATN (Fig. 2A, B). As with the wild type mice, the number of BrdU-labeled cells was increased in the DG of mice that received high frequency stimulation of the ATN (HF group): a 69% increase ($p=0.0074$) over the NF group and a 55% increase ($p=0.0139$) over the LF group; the difference between the LF and NF groups was not statistically significant (Fig. 2C). In all cases, BrdU-labeled cells were located in the SGZ, with rare cells found in the hilus (Fig. 2D-F). The stimulation-induced increase was restricted to the DG and was not seen in the SVZ. Together, the experiments with BrdU-labeling show that high frequency stimulation of ATN specifically increases cell division in the DG (Figs. 1, 2).

We next determined the class of progenitor cells targeted by high frequency stimulation by applying the scheme of the neuronal differentiation cascade in the DG that we have previously elaborated (Encinas and Enikolopov, 2008; Encinas et al., 2006; Enikolopov and Overstreet-Wadiche, 2007) and following the changes in individual classes of neural progenitors in our reporter Nestin-CFPnuc mice. In these animals, Nestin-CFPnuc-positive cells include quiescent neural progenitors, (QNPs) which act as adult hippocampal stem cells, and amplifying neural progenitors (ANPs) which are generated trough asymmetric division of QNPs. QNPs exhibit a radial glia-like morphology with a single long apical process that stains strongly for GFAP, whereas ANPs have short thin horizontal processes and do not stain for GFAP (Encinas et al., 2006; Enikolopov and Overstreet-Wadiche, 2007; Kempermann et al., 2004; Kronenberg et al., 2003; Seri et al., 2001). In our experiments, the total number of Nestin-CFPnuc cells was slightly, but not significantly, increased in the DG of HF animals; the vast majority of these cells were located in the SGZ (Fig. 3A-D, G,H). However, when these cells were classified as QNP or ANP using GFAP staining, it became obvious that the number of QNP did not change after high frequency stimulation of the ATN, whereas the number of ANPs was increased by 81% ($p=0.0017$) in the HF group over the NF group and by 64% ($p=0.0046$) over the LF group (Fig. 3E-H); again, there was no significant difference between the LF and NF groups (note that at the examined age, 2 months, QNPs largely outnumbers ANPs and the increase in the number of ANPs is not enough to significantly affect the total number of Nestin-CFPnuc cells).

High frequency stimulation of the ATN increases proliferation of ANPs but not asymmetrical division of QNPs

The increase in ANPs after high frequency stimulation can be explained both by augmented asymmetric divisions of QNPs or by augmented symmetric divisions of ANPs. These possibilities can be distinguished by determining the number of BrdU-labeled cells of each class, the mitotic index (the fraction of BrdU-labeled cells among the total number of cells in the given class), and the fraction of BrdU-labeled cells of a given class among the total number of BrdU-labeled cells. We used triple immunolabeling to identify the dividing progenitors, staining for Nestin-CFPnuc to visualize all progenitors, for GFAP to distinguish between QNP and ANP, and for BrdU to determine the number of dividing cells within each class (Fig. 4). The number of BrdU-labeled QNPs did not change in the HF as compared to the LF or NF groups (Fig. 4A), whereas the number of BrdU-labeled ANPs in the HF group was 81% higher than in the NF group ($p=0.0011$) and 63% higher than in the LF group ($p=0.0027$), with no significant difference between the LF and NF groups (Fig. 4B); furthermore, the clusters of ANPs in the SGZ appeared larger in the HF mice (Fig. 4C,H).

The mitotic index did not change in either the QNP or the ANP populations (Fig. 4M,N). The fraction of BrdU-labeled progenitors among the total number of BrdU-labeled cells did not change for the ANP in either of the experimental groups (Fig. 4P), whereas for the QNPs it decreased by 39% and 43% in the HF group as compared to the NF ($p=0.0021$) or the LF ($p=0.0016$) groups, respectively (Fig. 4O) (this decrease is due to the increase in the total number of BrdU-labeled cells). These results indicate that high frequency stimulation increased the number of dividing ANPs; that the representation among labeled cells was shifted towards the ANPs; and that the rate of division of QNP or ANP cells did not change after stimulation. These results also suggest that high frequency stimulation did not increase QNP division. Note that a similar result may have been observed if QNPs underwent an immediate transient increase in asymmetric divisions, giving rise to additional ANPs and then rapidly returning to their basal state by the time of analysis; however, such increase has not been observed in our previous experiments (Toda et al., 2008) (a caveat is that only a fraction of all BrdU-labeled cells in the SGZ is represented by QNPs and therefore a transient increase in QNPs may have been below the level of detection; note, however, that in similar experiments a difference of only 12% was detected with the statistical power of 0.8; data not shown). Taken together with the observed increase in the total number of ANPs, these data suggest that high frequency stimulation selectively increases symmetric divisions of ANPs.

This conclusion was further tested when we analyzed the classes of precursors derived from the ANPs. ANPs evolve into migrating post-mitotic precursors that slowly mature into granule neurons of the DG and can be further sub-categorized according to morphological criteria and expression of specific markers (Encinas et al., 2006; Kempermann et al., 2004; Seri et al., 2004). These postmitotic precursor classes, the neuroblasts type 1 (NB1) and type 2 (NB2); and immature neurons (INs), can be distinguished by morphological criteria and expression of specific markers (Fig. 5A-D) (Encinas et al., 2006; Kempermann et al., 2004; Seri et al., 2004). NB1 and NB2 cells are located along the SGZ. NB1 lack prolongationos or they are short and horizontal, whereas the more advanced NB2 extend longer oblique neurites into the GCL and very often contact the soma of the QNP and ANP cells (Fig. 5A-D,I,J). The soma of the INs can also be found in the SGZ, but the majority of these cells is already inserted into the GCL (Fig. 5D,I,J). INs extend a principal apical dendrite that ramifies and reaches the molecular layer. There was no significant change in the total number of neuroblasts (identified by the expression of PSA-NCAM) (Fig. 5E); however, the number of the earliest, least differentiated neuroblasts (NBs1) was increased in the HF group by 34% compared to the NF groups ($p=0.035$) and 41% compared to the LF group ($p=0.041$) (Fig. 5F). The number of more advanced neuroblasts (NB2s and immature neurons, showed no change (Fig. 5G,H). When considered together with the increased number of ANPs, such changes are expected if stimulation affects symmetric divisions of ANPs (i.e., producing more ANPs, part of which proceeds towards further differentiation within the framework of the treatment-labeling protocol) rather than asymmetric divisions of ANPs (i.e., ANPs producing more neuroblasts, with their own number staying the same). These results confirm our conclusion that stimulation of the ATN specifically augments symmetric divisions of ANPs in the adult DG.

High frequency stimulation of the ATN increases the generation of new neurons in the adult DG

To determine if the changes in proliferation of ANPs induced by stimulation of the ATN were later translated into an increase in the number of new neurons (Fig. 6), we analyzed the animals 30 days after the BrdU labeling. The number of $BrdU^+$ cells was increased in the DG of the animals of the HF group, 45% higher than in the NF group ($p=0.0137$) and 58% higher than in the LF group ($p=0.0114$; Fig. 6A). The number of new neurons ($BrdU^+$ cells

co-labeled with the neuronal marker NeuN; Fig. 6B-G) was also increased in the HF animals, by 53% compared to the NF animals (p=0.0136), and by 57% compared to the LF animals (p=0.0105; Fig. 6B); the majority of these neurons were localized to the GCL (Fig. 6D-G). The proportion of the newborn neurons to the total newly generated cells was not altered in either group (Fig. 6C), indicating that the stimulation-induced increase did not change the neuronal fate of the progenitors. We did not detect any changes in the total number of neural progenitors or in the number of QNPs or ANPs (Fig. 6H-L). These results indicate that high frequency stimulation of the ATN causes a transient increase in the number of stem and progenitor cells resulting in increased number of new neurons.

Discussion

Together, our results indicate that DBS-like high frequency stimulation of the ATN increases symmetric division of a defined class of neural progenitor in the SGZ of the DG, the transient amplifying neural progenitors (ANPs), and that this effect is later manifested as an increased number of new neurons in the granular layer of the DG. This class of progenitors is also targeted by the antidepressant fluoxetine (Encinas et al., 2006) and by physical exercise (Hodge et al., 2008), demonstrated in the same model. Thus, symmetric division of the ANPs may be the key step for the regulation of cell proliferation and neurogenesis in the DG, a common target on which pro-neurogenic stimuli of different nature (electrical, chemical, physiological) converge to increase the number of new granule cells.

Given the link between the changes in hippocampal neurogenesis and mood regulation (Drew and Hen, 2007; Santarelli et al., 2003; Warner-Schmidt and Duman, 2006; Zhao et al., 2008), it is possible that such diverse treatments as SSRI antidepressants, running, and DBS converge on the same neurogenic target in the DG and lead to comparable behavioral reactions. Furthermore, it is possible that these treatments, in addition to their effect of cell division, may also affect maturation (e.g., dendritic complexity, the number of synapses, and synaptic plasticity (Wang et al., 2008) of young and old (pre-existing) neurons; it is also conceivable that changes in the number and complexity of new neurons complement each other and contribute to the net effect of therapies and treatments that affect mood.

DBS of the anterior thalamus has been successfully applied to treat patients with epilepsy (Andrade et al., 2006; Kerrigan et al., 2004). Furthermore, DBS of different target regions has been successfully applied to patients with treatment-resistant depression (Bewernick et al.,; Jimenez et al., 2007; Lozano et al., 2008; Malone et al., 2009; Mayberg et al., 2005; Schlaepfer et al., 2008). It is conceivable that increased hippocampal neurogenesis contributed to the effects of these therapeutic interventions.

The position of the hippocampus in the limbic circuitry through which it may be influenced by the ATN, the anterior cingulate cortex, the limbic territory of the internal pallidal segments, and the ventral striatum (each of which has been a focal point for the therapeutic application of DBS), makes hippocampal neurogenesis a particularly relevant subject for investigating the effects of DBS. More generally, the demonstrated stimulation-proliferation coupling raises the possibility that DBS of the subcallosal cingulum (Mayberg et al., 2005) and other components of the limbic circuitry, e.g., the entorhinal cortex, septal region, or amygdala may be effective for inducing changes in hippocampal neurogenesis. Conversely, changes in the hippocampal neurogenesis may be used as a sensitive readout for the stimulation of the relevant components of the circuitry and for predicting the sites of DBS that may be effective for treating neuropsychiatric disorders.

Acknowledgments

We thank Tatyana Michurina, Stephen Hearn, Lisa Bianco and Jodi Coblentz for help with the experiments; and Amanda Sierra, Natalia Peunova, and Julian Banerji for the critical reading of the manuscript and helpful discussions. This work was supported by grants from National Institute of Mental Health (MH081258), New York State Stem Cell Science (NYSTEM 57850205), National Alliance for Research on Schizophrenia and Depression (NARSAD), The Seraph Foundation, The Ira Hazan Foundation, The Robertson Foundation, Cody Center for Autism and Developmental Disabilities, and Hope for Depression Foundation to G.E. J.M.E. is recipient of a NARSAD Young Investigator Award.

Support: National Institute of Mental Health (MH081258), New York State Stem Cell Science (NYSTEM 57850205), National Alliance for Research on Schizophrenia and Depression (NARSAD), The Seraph Foundation, The Ira Hazan Foundation, The Robertson Foundation, Cody Center for Autism and Developmental Disabilities, and Hope for Depression Foundation.

References

Andrade DM, Zumsteg D, Hamani C, Hodaie M, Sarkissian S, Lozano AM, Wennberg RA. Long-term follow-up of patients with thalamic deep brain stimulation for epilepsy. Neurology. 2006; 66(10): 1571–1573. [PubMed: 16540602]

Bewernick BH, Hurlemann R, Matusch A, Kayser S, Grubert C, Hadrysiewicz B, Axmacher N, Lemke M, Cooper-Mahkorn D, Cohen MX, Brockmann H, Lenartz D, Sturm V, Schlaepfer TE. Nucleus accumbens deep brain stimulation decreases ratings of depression and anxiety in treatment-resistant depression. Biol Psychiatry. 67(2):110–116. [PubMed: 19914605]

Drew MR, Hen R. Adult hippocampal neurogenesis as target for the treatment of depression. CNS Neurol Disord Drug Targets. 2007; 6(3):205–218. [PubMed: 17511617]

Encinas JM, Enikolopov G. Identifying and Quantitating Neural Stem and Progenitor Cells in the Adult Brain. Methods Cell Biol. 2008; 85C:243–272. [PubMed: 18155466]

Encinas JM, Vaahtokari A, Enikolopov G. Fluoxetine targets early progenitor cells in the adult brain. Proc Natl Acad Sci U S A. 2006; 103(21):8233–8238. [PubMed: 16702546]

Enikolopov, G.; Overstreet-Wadiche, L. Transgenic reporter lines for studying adult neurogenesis. In: Gage, F.; K, G.; Song, H., editors. Adult Neurogenesis. CSHL Press; 2007.

Franklin, KBJ.; Paxinos, G. The mouse brain in stereotaxic coordinates. San Diego: Academic Press; 1997. p. xxiip. 187ca.

Gabriels L, Cosyns P, Nuttin B, Demeulemeester H, Gybels J. Deep brain stimulation for treatment-refractory obsessive-compulsive disorder: psychopathological and neuropsychological outcome in three cases. Acta Psychiatr Scand. 2003; 107(4):275–282. [PubMed: 12662250]

Gao X, Enikolopov G, Chen J. Moderate traumatic brain injury promotes proliferation of quiescent neural progenitors in the adult hippocampus. Exp Neurol. 2009; 219(2):516–523. [PubMed: 19615997]

Greenberg BD, Gabriels LA, Malone DA Jr, Rezai AR, Friehs GM, Okun MS, Shapira NA, Foote KD, Cosyns PR, Kubu CS, Malloy PF, Salloway SP, Giftakis JE, Rise MT, Machado AG, Baker KB, Stypulkowski PH, Goodman WK, Rasmussen SA, Nuttin BJ. Deep brain stimulation of the ventral internal capsule/ventral striatum for obsessive-compulsive disorder: worldwide experience. Mol Psychiatry. 2010; 15(1):64–79. [PubMed: 18490925]

Guillery RW. On counting and counting errors. J Comp Neurol. 2002; 447(1):1–7. [PubMed: 11967890]

Hamani C, McAndrews MP, Cohn M, Oh M, Zumsteg D, Shapiro CM, Wennberg RA, Lozano AM. Memory enhancement induced by hypothalamic/fornix deep brain stimulation. Ann Neurol. 2008; 63(1):119–123. [PubMed: 18232017]

Hodge RD, Kowalczyk TD, Wolf SA, Encinas JM, Rippey C, Enikolopov G, Kempermann G, Hevner RF. Intermediate progenitors in adult hippocampal neurogenesis: Tbr2 expression and coordinate regulation of neuronal output. J Neurosci. 2008; 28(14):3707–3717. [PubMed: 18385329]

Houeto JL, Karachi C, Mallet L, Pillon B, Yelnik J, Mesnage V, Welter ML, Navarro S, Pelissolo A, Damier P, Pidoux B, Dormont D, Cornu P, Agid Y. Tourette's syndrome and deep brain stimulation. J Neurol Neurosurg Psychiatry. 2005; 76(7):992–995. [PubMed: 15965209]

Jimenez F, Velasco F, Salin-Pascual R, Velasco M, Nicolini H, Velasco AL, Castro G. Neuromodulation of the inferior thalamic peduncle for major depression and obsessive compulsive disorder. Acta Neurochir Suppl. 2007; 97(Pt 2):393–398. [PubMed: 17691327]

Kempermann G, Jessberger S, Steiner B, Kronenberg G. Milestones of neuronal development in the adult hippocampus. Trends Neurosci. 2004; 27(8):447–452. [PubMed: 15271491]

Kerrigan JF, Litt B, Fisher RS, Cranstoun S, French JA, Blum DE, Dichter M, Shetter A, Baltuch G, Jaggi J, Krone S, Brodie M, Rise M, Graves N. Electrical stimulation of the anterior nucleus of the thalamus for the treatment of intractable epilepsy. Epilepsia. 2004; 45(4):346–354. [PubMed: 15030497]

Kopell BH, Greenberg B, Rezai AR. Deep brain stimulation for psychiatric disorders. J Clin Neurophysiol. 2004; 21(1):51–67. [PubMed: 15097294]

Kronenberg G, Reuter K, Steiner B, Brandt MD, Jessberger S, Yamaguchi M, Kempermann G. Subpopulations of proliferating cells of the adult hippocampus respond differently to physiologic neurogenic stimuli. J Comp Neurol. 2003; 467(4):455–463. [PubMed: 14624480]

Lozano AM, Hamani C. The future of deep brain stimulation. J Clin Neurophysiol. 2004; 21(1):68–69. [PubMed: 15097295]

Lozano AM, Mayberg HS, Giacobbe P, Hamani C, Craddock RC, Kennedy SH. Subcallosal cingulate gyrus deep brain stimulation for treatment-resistant depression. Biol Psychiatry. 2008; 64(6):461–467. [PubMed: 18639234]

Malone DA Jr, Dougherty DD, Rezai AR, Carpenter LL, Friehs GM, Eskandar EN, Rauch SL, Rasmussen SA, Machado AG, Kubu CS, Tyrka AR, Price LH, Stypulkowski PH, Giftakis JE, Rise MT, Malloy PF, Salloway SP, Greenberg BD. Deep brain stimulation of the ventral capsule/ventral striatum for treatment-resistant depression. Biol Psychiatry. 2009; 65(4):267–275. [PubMed: 18842257]

Mayberg HS, Lozano AM, Voon V, McNeely HE, Seminowicz D, Hamani C, Schwalb JM, Kennedy SH. Deep brain stimulation for treatment-resistant depression. Neuron. 2005; 45(5):651–660. [PubMed: 15748841]

Mignone JL, Kukekov V, Chiang AS, Steindler D, Enikolopov G. Neural stem and progenitor cells in nestin-GFP transgenic mice. J Comp Neurol. 2004; 469(3):311–324. [PubMed: 14730584]

Park JH, Enikolopov G. Transient elevation of adult hippocampal neurogenesis after dopamine depletion. Exp Neurol. 2010; 222(2):267–276. [PubMed: 20079351]

Peterson DDA. Quantitative histology using confocal microscopy: implementation of unbiased stereology procedures. Methods. 1999; 18(4):493–507. [PubMed: 10491280]

Santarelli L, Saxe M, Gross C, Surget A, Battaglia F, Dulawa S, Weisstaub N, Lee J, Duman R, Arancio O, Belzung C, Hen R. Requirement of hippocampal neurogenesis for the behavioral effects of antidepressants. Science. 2003; 301(5634):805–809. [PubMed: 12907793]

Schiff ND, Giacino JT, Kalmar K, Victor JD, Baker K, Gerber M, Fritz B, Eisenberg B, Biondi T, O'Connor J, Kobylarz EJ, Farris S, Machado A, McCagg C, Plum F, Fins JJ, Rezai AR. Behavioural improvements with thalamic stimulation after severe traumatic brain injury. Nature. 2007; 448(7153):600–603. [PubMed: 17671503]

Schlaepfer TE, Cohen MX, Frick C, Kosel M, Brodesser D, Axmacher N, Joe AY, Kreft M, Lenartz D, Sturm V. Deep brain stimulation to reward circuitry alleviates anhedonia in refractory major depression. Neuropsychopharmacology. 2008; 33(2):368–377. [PubMed: 17429407]

Seri B, Garcia-Verdugo JM, Collado-Morente L, McEwen BS, Alvarez-Buylla A. Cell types, lineage, and architecture of the germinal zone in the adult dentate gyrus. J Comp Neurol. 2004; 478(4):359–378. [PubMed: 15384070]

Seri B, Garcia-Verdugo JM, McEwen BS, Alvarez-Buylla A. Astrocytes give rise to new neurons in the adult mammalian hippocampus. J Neurosci. 2001; 21(18):7153–7160. [PubMed: 11549726]

Toda H, Hamani C, Fawcett AP, Hutchison WD, Lozano AM. The regulation of adult rodent hippocampal neurogenesis by deep brain stimulation. J Neurosurg. 2008; 108(1):132–138. [PubMed: 18173322]

Vandewalle V, van der Linden C, Groenewegen HJ, Caemaert J. Stereotactic treatment of Gilles de la Tourette syndrome by high frequency stimulation of thalamus. Lancet. 1999; 353(9154):724. [PubMed: 10073521]

Wang JW, David DJ, Monckton JE, Battaglia F, Hen R. Chronic fluoxetine stimulates maturation and synaptic plasticity of adult-born hippocampal granule cells. J Neurosci. 2008; 28(6):1374–1384. [PubMed: 18256257]

Warner-Schmidt JL, Duman RS. Hippocampal neurogenesis: opposing effects of stress and antidepressant treatment. Hippocampus. 2006; 16(3):239–249. [PubMed: 16425236]

Wichmann T, Delong MR. Deep brain stimulation for neurologic and neuropsychiatric disorders. Neuron. 2006; 52(1):197–204. [PubMed: 17015236]

Yamamoto T, Katayama Y, Oshima H, Fukaya C, Kawamata T, Tsubokawa T. Deep brain stimulation therapy for a persistent vegetative state. Acta Neurochir Suppl. 2002; 79:79–82. [PubMed: 11974994]

Zhao C, Deng W, Gage FH. Mechanisms and functional implications of adult neurogenesis. Cell. 2008; 132(4):645–660. [PubMed: 18295581]

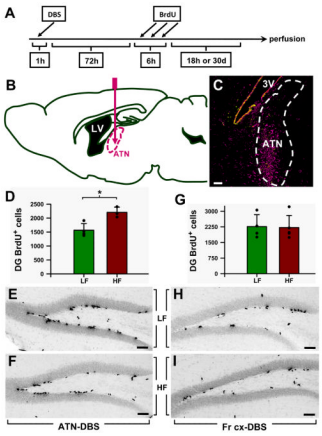

Figure 1. Specificity of the ATN stimulation in increasing cell proliferation in the adult mouse DG

A: Scheme of the protocol detailed in the Material and Methods section.

B: Scheme of the pathway followed by the electrode to reach the anterior thalamic nuclei (ATN) in the mouse brain.

C: Glial activation (identified by vimentin immunostaining) was used for *post mortem* confirmation that the electrode was inserted into the correct area. The image is from a sagittal slice of the brain after applying stimulation. Vimentin immunostaining is seen as a magenta signal and the Nestin-CFPnuc signal as green. 3V: third ventricle.

D: Stimulation applied to the ATN increases cell proliferation in the DG of adult wild-type mice. In the control LF (low frequency) group, the electrode was inserted in the ATN and the electrical current was applied at 10 Hz; in the experimental group (the HF group), the current was applied at 130Hz. The stereological quantification of the $BrdU^+$ cells showed significantly increased cell proliferation (by 40%, p=0.0125) in the DG of the HF group.

E,F: Representative images of the DG from an LF (**E**) and a HF (**F**) mouse after immunostaining for BrdU.

G: To test the specificity of the ATN stimulation in increasing DG cell proliferation, in a separate group of animals the frontal associative area of the cortex (FrA) was targeted. Quantification of the $BrdU^+$ cells in the DG showed that there was no difference in cell proliferation between the LF and the HF groups.

H,I: Representative pictures of the DG of LF (**H**) and HF (**I**) mice after BrdU immunostaining. Data are shown as mean±s.e.m (n=4 mice for all groups, represented by black dots here and in other figures). *p<0.05. Scale bar is 50μm in all pictures.

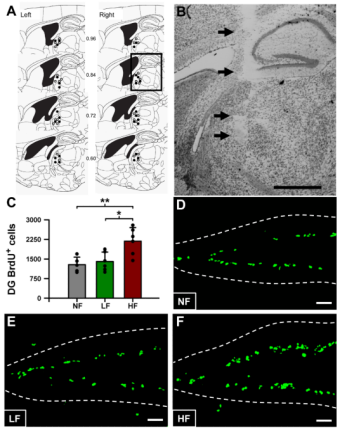

Figure 2. High frequency stimulation of the ATN increases the number of dividing cells in the DG of adult Nestin-CFPnuc mice

A: Location of electrodes in the anterior thalamic nuclear complex of animals undergoing electrical stimulation. Schematic representation of sagittal brain sections depicting the region in which the tips of the electrodes were identified. Each circle represents a single electrode of C57BL/6 and Nestin-CFPnuc mice undergoing bilateral high (black) or low frequency stimulation (gray) (total of 28 animals). Numbers in between plates denote distance from the midline. Left and right denote left and right hemispheres. Figure is modified and reprinted from “The mouse brain in stereotaxic coordinates” (Franklin and Paxinos, 1997).

B: Photomicrograph of a typical ATN electrode tract (arrows). The region of histological analysis corresponds to the square in the bottom plate of Fig. 2A. Scale bar is 1 mm.

C: High frequency stimulation of the ATN increases the number of BrdU cell in the DG of adult Nestin-CFPnuc mice.

D-F: Representative confocal microscopy images of the DG from NF (**D**), LF (**E**), and HF (**F**) mice, after BrdU immunostaining. Scale bar is 50μm.

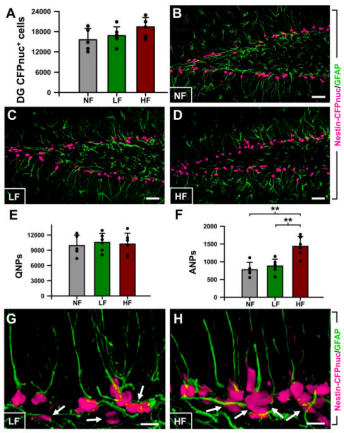

Figure 3. High frequency stimulation of the ATN increases the number of ANPs in the adult DG

A: Quantification of the number of Nestin-CFPnuc cells.

B-D: Representative confocal microscopy images of the DG from NF (**B**), LF (**C**), and HF (**D**) mice after CFP (magenta) and GFAP (green) staining.

E: Quantification of the number of QNPs, Nestin-CFPnuc$^+$ cells with apical GFAP$^+$ process.

F: Quantification of the number of ANPs, Nestin-CFPnuc$^+$ cells without any GFAP$^+$ process.

G,H: Representative confocal microscopy images of the DG from LF (**G**), and HF (**H**) mice after CFP (magenta) and GFAP (green) staining, arrows showing dividing ANPs and larger clusters of ANPs induced by the stimulation of the ATN. Data are show as mean±s.e.m. (n=5 for the NF group and 6 for the LF and HF groups). *p<0.05. Scale bar is 10μm in **G,H** and 50μm in other pictures.

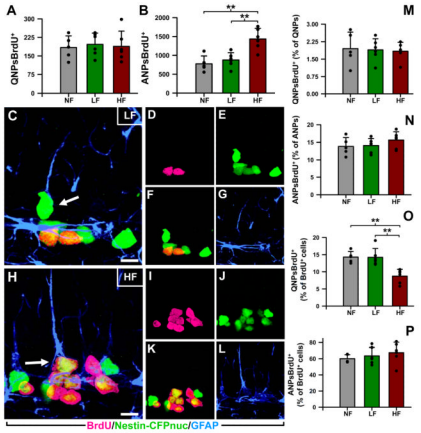

Figure 4. High frequency stimulation of the ATN increases the mitotic activity of ANPs

A: The number of QNPs immunostained for $BrdU^+$ did not change in any experimental group.

B: The number of ANPs immunostained for BrdU was significantly increased in the HF animals, demonstrating that they are proliferating more whereas the mitotic activity of the QNPs did not change.

C-L: Representative confocal microscopy images from DG sections of LF (**C-G**), and HF (**H-L**) animals. Anti-BrdU staining is shown in magenta (**D,I**), and anti-CFP staining is shown in green (**E,J**); the overlap is seen as yellow in (**F,K**). Anti-GFAP staining, to distinguish between the QNPs (arrows in **C,H**) and the ANPs is shown in blue (**G,L**). In the image from the HF animal, higher numbers of $BrdU^+$, ANPs, and $BrdU^+$ANPs as compared to the LF animals, are evident.

M,N: The relative proportion of $BrdU^+$QNPs within the QNP population (n) or $BrdU^+$ANPs within the ANP population were not altered in any group.

O,P: The relative proportion of $BrdU^+$QNPs within the population of $BrdU^+$ cells was significantly decreased in the HF as compared to the NF and LF groups (**P**); the decrease is due to the increase in $BrdU^+$ cells as the number of QNPs remains constant. The relative proportion of $BrdU^+$ANPs within the ANP population, however, was not affected by stimulation of the ATN (**P**). Data are shown as mean±s.e.m (n=5 mice for the NF group and 6 for LF and HF groups). **p<0.005, ***p<0.001. Scale bars are 10μm.

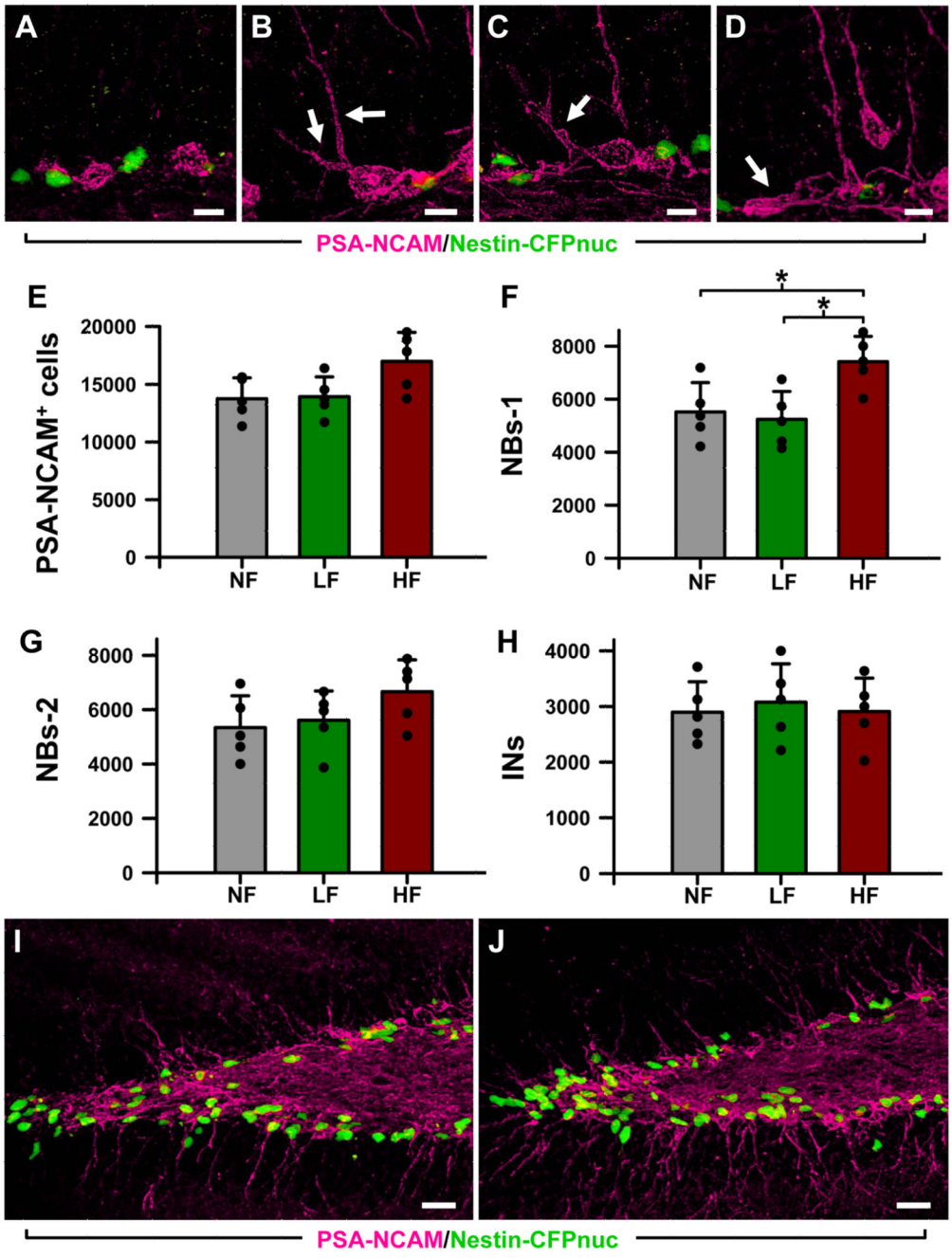

Figure 5. High frequency stimulation of the ATN induces changes in the number of neuroblasts

A: Type-1 neuroblasts (NB1s), located along the SGZ, with small round soma and short thin horizontal processes. **B,C:** Type-2 neuroblasts (NB2s) cells located along the SGZ and with horizontal and oblique processes entering the GCL (arrows).

D: Immature neurons (INs), located in the SGZ and the GCL, with a single apical process crossing the GCL. An NB1 cell can also be observed (arrow).

E-H: The overall number of neuroblasts (PSA-CAM$^+$ cells) is slightly higher in the HF animals. Within that group, the number of NB1s is significantly increased (**F**), whereas the number of NB2s (**G**) and INs (**H**) is not changed. I and J Representative confocal microscopy images of sections from the DG of LF (**I**) and HF (**J**) mice showing the location

of the neuroblasts (PSA-NCAM$^+$ cells, in magenta) and neuroprogenitors (CFPnuc$^+$ cells, in green). Both types of cells are in close apposition. Data are shown as mean ± s.e.m (n = 5 mice for the NF group, and 6 for the LF and HF groups, animals represented by black dots). * $p < 0.05$. Scale bar is 5 μm in (**A-D**) and 25 μm in (**I, J**).

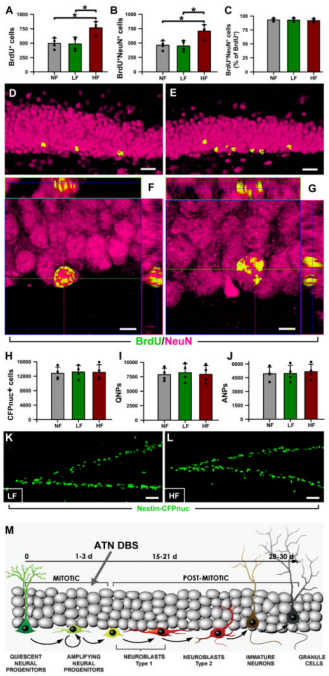

Figure 6. High frequency stimulation of the ATN increases neurogenesis in the adult mouse DG

A: The number of $BrdU^+$ cells, measured 1 month after BrdU administration, was significantly increased in the DG of the HF mice.

B: The number of newly-generated neurons ($BrdU^+NeuN^+$cells) was increased as well.

C: The proportion of neurons ($NeuN^+BrdU^+$) within the population of new-born cells ($BrdU^+$ cells) was not affected by the stimulation of the ATN.

D,E: Representative confocal microscopy images of the DG from LF (**D**), and HF (**E**) animals. The $BrdU^+$ cells are located in the lower section of the granule cell layer and are found in higher number in the HF animals (**E**).

F,G: Orthogonal projections, at high magnification, of $NeuN^+BrdU^+$ cells from LF (**F**) and HF (**G**) mice, showing their neuronal fate of new-born cells. Data are shown as mean±s.e.m. (n=4 mice in all groups) *p<0.05. Scale bar is 20μm in (**D,E**) and 5μm in (**F, G**).

H-J: The total number of neuroprogenitors ($Nestin\text{-}CFPnuc^+$ cells) is similar for all the animal groups one month after the BrdU administration (**H**). The same is true for the number of QNPs (**I**) and ANPs (**J**).

K,L: Representative images of the DG from the LF (**K**) and HF (**L**) animals after immunostaining for CFP. No differences were found in terms of numbers, location, or morphology of the DG neuroprogenitors. Data are show as mean±s.e.m. (n=4 mice in all groups). *p<0.05. Scale bar is 20μm in (**D,E**), 5μm in (**F,G**), and 50μm in (**K,L**).

M. Schematics of the differentiation cascade in the DG and progenitor population targeted by DBS of the ATN. Basic scheme of neurogenesis corresponds to that in (Encinas et al., 2006).

Table 1

Primary antibodies used in the current study

Antigen	Immunogen	Host/Isotype	Working dilution	Source	Catalog No.
BrdU	5-Bromo-deoxy-uridine	Rat/IgG2a	1:400	AbD Serotec	OBT0030
GFAP	GFAP purified from human brain	Rabbit/IgG	1:1000	Sigma	G 9269
GFP	Purified recombinant green fluorescent protein	Chicken/IgY	1:500	Aves Labs	GFP-1020
NeuN	Purified cell nuclei from mouse brain	Mouse/IgG1	1:800	Chemicon	MAB377
PSA-NCAM	Viable Meningococcus group B (strain 355)	Mouse/IgM	1:400	Chemicon	MAB5324